Neural Operator: Graph Kernel Network for Partial Differential Equations

Abstract

The classical development of neural networks has been primarily for mappings between a finite-dimensional Euclidean space and a set of classes, or between two finite-dimensional Euclidean spaces. The purpose of this work is to generalize neural networks so that they can learn mappings between infinite-dimensional spaces (operators). We formulate approximation of the infinite-dimensional mapping by composing nonlinear activation functions and a class of integral operators. The kernel integration is computed by message passing on graph networks. This approach has substantial practical consequences which we will illustrate in the context of mappings between input data to partial differential equations (PDEs) and their solutions. In this context, such learned networks can generalize among different approximation methods for the PDE (such as finite difference or finite element methods) and among approximations corresponding to different underlying levels of resolution and discretization. Experiments confirm the purposed graph kernel network does have the desired properties and show competitive performance compared to the stat of the art solvers.

1 INTRODUCTION

There are numerous applications in which it is desirable to learn a mapping between Banach spaces. In particular, either the input or the output space, or both, may be infinite dimensional. The possibility of learning such mappings opens up a new class of problems in the design of neural networks, with widespread potential applicability. New ideas are required to build on traditional neural networks which are mappings from finite dimensional Euclidean spaces into classes, or into another finite-dimensional Euclidean space. We study the development of neural networks in the setting in which the input and output spaces comprise real-valued functions defined on a bounded open set D in $\mathbb{R}^d$.

1.1 Our Contributions

We introduce a new neural network architecture which is appropriate for the learning of mappings between spaces of functions defined on bounded open subsets of $\mathbb{R}^d$.

- Unlike existing methods, our approach is demonstrably able to share a single set of neural network parameters between methods based on different approximation methods and different grids.
- A Nyström extension connects the neural network on function space to families of GNNs on arbitrary, possibly unstructured, grids.
- The method is demonstrated to have competitive approximation accuracy, as shown in the experiments.
- The ability of transfer learning between different discretizations with one set of parameters .
- The ability of semi-supervised learning that learns from data at a few points and the generalizes to the whole domain.

These concepts are illustrated in the context of a family of elliptic PDEs prototypical of a number of problems arising throughout the sciences and engineering.

2 PROBLEM SETTING

Our goal is to learn a mapping between two infinite dimensional spaces by using a finite collection of observations of input-output pairs from this mapping: supervised learning. Let $\mathcal{A}$ and $\mathcal{U}$ be separable Banach spaces and $\mathcal{F}^\dagger : \mathcal{A} \to \mathcal{U}$ a (typically) non-linear map. Suppose we have observations $\{a_j, u_j\}_{j=1}^N$ where $a_j \sim \mu$ is an i.i.d. sequence from the probability measure μ supported on $\mathcal{A}$ and $u_j = \mathcal{F}^\dagger(a_j)$ is possibly corrupted with noise. We aim to build an approximation of $\mathcal{F}^\dagger$ by constructing a parametric map

$$\mathcal{F} : \mathcal{A} \times \Theta \to \mathcal{U} \tag{1}$$

for some finite-dimensional parameter space Θ and then choosing $\theta^\dagger \in \Theta$ so that $\mathcal{F}(\cdot, \theta^\dagger) \approx \mathcal{F}^\dagger$.

This a natural framework for learning in infinite-dimensions as one could define a cost functional $C : \mathcal{U} \times \mathcal{U} \to \mathbb{R}$ and seek a minimizer of the problem

$$\min_{\theta \in \Theta} \mathbb{E}_{a\sim\mu}[C(\mathcal{F}(a, \theta), \mathcal{F}^\dagger(a))]$$

which directly parallels the classical finite-dimensional setting [Vapnik, 1998]. Showing the existence of minimizers, in the infinite-dimensional setting, remains a challenging open problem. We will approach this problem in the test-train setting in which empirical approximations to the cost are used. We conceptualize our methodology in the infinite-dimensional setting. This means that all finite-dimensional approximations can share a common set of network parameters which are defined in the (approximation-free) infinite-dimensional setting. To be concrete we will consider infinite-dimensional spaces which are Banach spaces of real-valued functions defined on a bounded open set in $\mathbb{R}^d$. We then consider mappings $\mathcal{F}^\dagger$ which take input functions to a PDE and map them to solutions of the PDE, both input and solutions being real-valued functions on $\mathbb{R}^d$.

A common instantiation of the preceding problem is the approximation of the second order elliptic PDE

$$\begin{aligned} -\nabla \cdot (a(x)\nabla u(x)) = f(x), \quad & x \in D \\ u(x) = 0, \quad & x \in \partial D \end{aligned} \tag{2}$$

for some bounded, open set $D \subset \mathbb{R}^d$ and a fixed function $f \in L^2(D; \mathbb{R})$. This equation is prototypical of PDEs arising in numerous applications including hydrology [Bear and Corapcioglu, 2012] and elasticity [Antman, 2005]. For a given $a \in \mathcal{A} = L^\infty(D; \mathbb{R}^+) \cap L^2(D; \mathbb{R}^+)$, equation (2) has a unique weak solution $u \in \mathcal{U} = H_0^1(D; \mathbb{R})$ [Evans, 2010] and therefore we can define the solution operator $\mathcal{F}^\dagger$ as the map $a \mapsto u$. Note that while the PDE (2) is linear, the solution operator $\mathcal{F}^\dagger$ is not.

Since our data a_j and u_j are , in general, functions, to work with them numerically, we assume access only to point-wise evaluations. To illustrate this, we will continue with the example of the preceding paragraph. To this end let $P_K = \{x_1, \dots, x_K\} \subset D$ be a K-point discretization of the domain D and assume we have observations $a_j|_{P_K}, u_j|_{P_K} \in \mathbb{R}^K$, for a finite collection of input-output pairs indexed by j. In the next section, we propose a kernel inspired graph neural network architecture which, while trained on the discretized data, can produce an answer $u(x)$ for any $x \in D$ given a new input $a \sim \mu$. That is to say that our approach is independent of the discretization P_K and therefore a true function space method; we verify this claim numerically by showing invariance of the error as $K \to \infty$. Such a property is highly desirable as it allows a transfer of solutions between different grid geometries and discretization sizes.

3 GRAPH KERNEL NETWORK

We propose a graph kernel neural network for the solution of the problem outlined in section 2. As a guiding principle of our architecture, we take the following example. Let $\mathcal{L}_a$ be a differential operator depending on a parameter $a \in \mathcal{A}$ and consider the PDE

$$\begin{aligned} (\mathcal{L}_a u)(x) = f(x), \quad & x \in D \\ u(x) = 0, \quad & x \in \partial D \end{aligned} \tag{3}$$

for a bounded, open set $D \subset \mathbb{R}^d$ and some fixed function f living in an appropriate function space determined by the structure of $\mathcal{L}_a$. The elliptic operator $\mathcal{L}_a \cdot = -\text{div}(a\nabla \cdot)$ from equation (2) is an example. Under fairly general conditions on $\mathcal{L}_a$ [Evans, 2010], we may define the Green's function $G : D \times D \to \mathbb{R}$ as the unique solution to the problem

$$\mathcal{L}_a G(x, \cdot) = \delta_x$$

where δ_x is the delta measure on $\mathbb{R}^d$ centered at x. Note that G will depend on the parameter a thus we will henceforth denote it as G_a. The solution to (3) can then be represented as

$$u(x) = \int_D G_a(x, y) f(y)\, dy. \tag{4}$$

Generally the Green's function is continuous at points $x \neq y$, for example, when $\mathcal{L}_a$ is uniformly elliptic [Gilbarg and Trudinger, 2015], hence it is natural to model it via a neural network. Guided by the representation (4), we propose the following iterative architecture for $t = 0, \dots, T-1$.

$$v_{t+1}(x) = \sigma\Big(W v_t(x) + \int_D \kappa_\phi(x, y, a(x), a(y)) v_t(y)\, \nu_x(dy) \Big) \tag{5}$$

where $\sigma : \mathbb{R} \to \mathbb{R}$ is a fixed function applied elementwise, ν_x is a fixed Borel measure for each $x \in D$ and $W \in \mathbb{R}^{n \times n}$, together with the parameters ϕ entering kernel $\kappa_\phi : \mathbb{R}^{2(d+1)} \to \mathbb{R}^{n \times n}$, are to be learned from data. We model κ_ϕ as a neural network mapping $\mathbb{R}^{2(d+1)}$ to $\mathbb{R}^{n \times n}$.

Discretization of the continuum picture may be viewed as replacing Borel measure ν_x by an empirical approximation based on the K grid points being used. In this setting we may view κ_ϕ as a $K \times K$ kernel block matrix, where each entry $\kappa_\phi(x, y)$ is itself a $n \times n$ matrix. Each block shares the same set of network parameters. This is the key to making a method which shares common parameters independent of the discretization used.

Finally we observe that, although we have focussed on neural networks mapping a to u, generalizations are possible, such as mapping f to u, or having non-zero boundary data g on ∂D and mapping g to u. More generally one can consider the mapping from (a, f, g) into u and use similar ideas. To illustrate ideas we will consider the mapping from f to u below (which is linear and for which an analytic solution is known) before moving on study the (nonlinear) mapping from a to u. Since in the setting f is fixed, our iterative kernel integration convoluted with representation v instead of f.

Algorithmic Framework. The initialization $v_0(x)$ to our network (5) can be viewed as the initial guess we make for the solution $u(x)$ as well as any other dependence we want to make explicit. A natural choice is to start with the coefficient $a(x)$ itself as well as the position in physical space x. This $(d+1)$-dimensional vector field is then lifted to a n-dimensional vector field, an operation which we may view as the first layer of the overarching neural network. This is then used as an initialization to the kernel neural network, which is iterated T times. In the final layer, we project back to the scalar field of interest with another neural network layer.

Due to the smoothing effect of the inverse elliptic operator in (2) with respect to the input data a (and indeed f when we consider this as input), we augment the initialization $(x, a(x))$ with a Gaussian smoothed version of the coefficients $a_\epsilon(x)$, together with their gradient $\nabla a_\epsilon(x)$. Thus we initialize with a $2(d+1)$-dimensional vector field. Throughout this paper the Gaussian smoothing is performed with a centred isotropic Gaussian with variance 5. The Borel measure ν_x is chosen to be the Lebesgue measure supported on a ball at x of radius r. Thus we have

$$v_0(x) = P(x, a(x), a_\epsilon(x), \nabla a_\epsilon(x)) + p \tag{6}$$

$$v_{t+1}(x) = \sigma\Big(W v_t(x) + \int_{B(x,r)} \kappa_\phi\big(x, y, a(x), a(y)\big) v_t(y)\, \mathrm{d}y \Big) \tag{7}$$

$$u(x) = Q v_T(x) + q \tag{8}$$

where $P \in \mathbb{R}^{n \times 2(d+1)}$, $p \in \mathbb{R}^n$, $v_t(x) \in \mathbb{R}^n$ and $Q \in \mathbb{R}^{1 \times n}$, $q \in \mathbb{R}$. The integration in (7) is approximated by a Monte Carlo sum via a message passing graph network with edge weights $(x, y, a(x), a(y))$. The choice of measure $\nu_x(\mathrm{d}y) = \mathbb{1}_{B(x,r)} \mathrm{d}y$ is two-fold: 1) it allows for more efficient computation and 2) it exploits the decay property of the Green's function.

Message Passing Graph Networks. Message passing graph networks comprise a standard architecture employing edge features [Gilmer et al., 2017]. If we properly construct the graph on the spatial domain D of the PDE, the kernel integration can be viewed as an aggregations of messages. Given node features $v_t(x) \in \mathbb{R}^n$, edge features $e(x, y) \in \mathbb{R}^{n_e}$, and a graph G, the message passing neural network with averaging aggregation is

$$v_{t+1}(x) = W v_t(x) + \frac{1}{|N(x)|} \sum_{y \in N(x)} \kappa_\phi\big(e(x, y)\big) v_t(y) \tag{9}$$

where $W \in \mathbb{R}^{n \times n}$, $N(x)$ is the neighborhood of x according to the graph, $\kappa_\phi\big(e(x, y)\big)$ is a neural network taking as input edge features and as output a matrix in $\mathbb{R}^{n \times n}$. In relation to (7), $e(x, y) = (x, y, a(x), a(y)) \in \mathbb{R}^{2(d+1)}$.

Graph Construction. To use the message passing framework (9), we need to design a graph which connects the physical domain D of the PDE. The nodes are chosen to be the K discretized spatial locations. Here we work on a standard uniform mesh, but there are many other possibilities such as finite-element triangulations. The edge connectivity is then chosen according to the integration measure in (7). In particular, each node $x \in \mathbb{R}^d$ is connected to all neighboring nodes which lie within the ball $B(x, r)$, defining the neighborhood set $N(x)$. Then for each neighbor $y \in N(x)$, we assign the edge weight $e(x, y) = (x, y, a(x), a(y))$. Equation (9) can then be viewed as a Monte Carlo approximation of (7). This local structure allows for more efficient computation while remaining invariant to mesh-refinement. Indeed, since the radius parameter r is chosen in physical space, the size of the set $N(x)$ grows as the disretization size K grows. This is a key feature which makes our methodology mesh-independent.

Nyström Approximation of the Kernel. While the aforementioned graph structure severely reduces the computational overhead of integrating over the entire domain D (corresponding to a fully-connected graph), the number of edges still scale like $\mathcal{O}(K^2)$. To overcome this, we employ a random Nyström-type approximation of the kernel. In particular, we uniformly sample $m \ll K$ nodes from the original graph, constructing a new random sub-graph. This process is repeated $l \in \mathbb{N}$ times, yielding l random sub-graphs each with m nodes. This can be thought of as a way of reducing the variance in the estimator. We use these sub-graphs when evaluating (9) during training which gives the more favorable scaling $\mathcal{O}(lm^2)$. Indeed, numerically we find that $l = 4$ and $m = 200$ is sufficient even when $K = 421^2 = 177,241$. In the evaluation phase, when we want the solution on a particular mesh geometry, we simply partition the mesh into sub-graphs each with m nodes and evaluate each separately.

We will now demonstrate the quality of this kernel approximation in a RHKS setting. A real Reproducing Kernel Hilbert Space (RKHS) $(\mathcal{H}, \langle\cdot,\cdot\rangle, \|\cdot\|)$ is a Hilbert space of functions $f : D \to \mathbb{R}$ where point-wise evaluation is a continuous linear functional, i.e. $|f(x)| \leq C\|f\|$ for some constant $C \geq 0$, independent of x. For every RHKS, there exists a unique, symmetric, positive definite kernel $\kappa : D \times D \to \mathbb{R}$, which gives the representation $f(x) = \langle f, \kappa(\cdot, x)\rangle$. Let $T : \mathcal{H} \to \mathcal{H}$ be a linear operator on $\mathcal{H}$ acting via the kernel

$$Tf = \int_{B(\cdot,r)} \kappa(\cdot, y) f(y) \nu(dy).$$

Let $T_m : \mathcal{H} \to \mathcal{H}$ be its m-point empirical approximation

$$T_m = \int_{B(\cdot,r)} \kappa(\cdot, y) f(y) \nu_m(dy)$$

hence

$$\nu_m(dy) = \frac{1}{m}\sum_{k=1}^{m} \delta_{y_k}(dy),$$

$$T_m f = \frac{1}{m}\sum_{k=1}^{m} \kappa(\cdot, y_k) f(y_k).$$

The error of this approximation achieves the Monte Carlo rate $O(m^{-1/2})$:

Proposition 1. *Suppose* $\mathbb{E}_{y\sim\nu}[\kappa(\cdot, y)^4] < \infty$ *then there exists a constant* $C \geq 0$ *such that*

$$\mathbb{E}\|T - T_m\|_{HS} \leq \frac{C}{\sqrt{m}}$$

where $\|\cdot\|_{HS}$ *denotes the Hilbert-Schmidt norm on operators acting on* $\mathcal{H}$.

4 EXPERIMENTS

In the following section, we compare kernel networks with different benchmarks on Darcy Equation. The network is trained and evaluated on the same full grid. The results are presented in Table 1. **NN** is a simple point-wise feedforward neural network. It is mesh-free, but perform badly due to lack of neighbor information. **FCN** is the state of the art neural network method based on Fully Convolution Network [Zhu and Zabaras, 2018]. It has a dominating performance for small grids $s = 61$. But fully convolution networks are mesh-dependent and therefore their error grows when moving to a larger grid. **PCA+NN** is an instantiation of the methodology proposed in [Bhattacharya et al., 2020]: using PCA as an autoencoder on both the input and output data and interpolating the latent spaces with a neural network. The method provably obtains mesh-independent error and can learn purely from data, however the solution can only be evaluated on the same mesh as the training data. **RBM** is the classical Reduced Basis Method (using a PCA basis), which is widely used in application and provably obtains mesh-independent error [DeVore, 2014]. It has the best performance but the solutions can only be evaluated on the same mesh as the training data and one needs knowledge of the PDE to employ it. **KernelGNN** stands for our graph kernel network. It enjoys competitive performance against all other methods while being able to generalize to different mesh geometries.

Table 1: Scaling of different network architectures

Networks	**141**	**211**	**421**
NN	0.1716	0.1716	0.1716
FCN	0.0493	0.0727	0.1097
PCA+NN	0.0298	0.0298	0.0299
RBM	0.0251	0.0255	0.0259
KernelGNN	0.0332	0.0342	0.0369

References

[Antman, 2005] Antman, S. S. (2005). *Problems In Nonlinear Elasticity*. Springer.

[Bear and Corapcioglu, 2012] Bear, J. and Corapcioglu, M. Y. (2012). *Fundamentals of transport phenomena in porous media*, volume 82. Springer Science & Business Media.

[Bhattacharya et al., 2020] Bhattacharya, K., Kovachki, N. B., and Stuart, A. M. (2020). Model reduction and neural networks for parametric pde(s). *preprint*.

[DeVore, 2014] DeVore, R. A. (2014). *Chapter 3: The Theoretical Foundation of Reduced Basis Methods*.

[Evans, 2010] Evans, L. C. (2010). *Partial Differential Equations*, volume 19. American Mathematical Soc.

[Gilbarg and Trudinger, 2015] Gilbarg, D. and Trudinger, N. S. (2015). *Elliptic partial differential equations of second order*. springer.

[Gilmer et al., 2017] Gilmer, J., Schoenholz, S. S., Riley, P. F., Vinyals, O., and Dahl, G. E. (2017). Neural message passing for quantum chemistry. In *Proceedings of the 34th International Conference on Machine Learning-Volume 70*, pages 1263–1272. JMLR. org.

[Vapnik, 1998] Vapnik, V. N. (1998). *Statistical Learning Theory*. Wiley-Interscience.

[Zhu and Zabaras, 2018] Zhu, Y. and Zabaras, N. (2018). Bayesian deep convolutional encoderdecoder networks for surrogate modeling and uncertainty quantification. *Journal of Computational Physics*, 366:415 – 447.

Neural Operator: Graph Kernel Network for Partial Differential Equations

Abstract

The classical development of neural networks has been primarily for mappings between a finite-dimensional Euclidean space and a set of classes, or between two finite-dimensional Euclidean spaces. The purpose of this work is to generalize neural networks so that they can learn mappings between infinite-dimensional spaces (operators). The key innovation in our work is that a single set of network parameters, within a carefully designed network architecture, may be used to describe mappings between infinite-dimensional spaces *and* between different finite-dimensional approximations of those spaces. We formulate approximation of the infinite-dimensional mapping by composing nonlinear activation functions and a class of integral operators. The kernel integration is computed by message passing on graph networks. This approach has substantial practical consequences which we will illustrate in the context of mappings between input data to partial differential equations (PDEs) and their solutions. In this context, such learned networks can generalize among different approximation methods for the PDE (such as finite difference or finite element methods) and among approximations corresponding to different underlying levels of resolution and discretization. Experiments confirm the purposed graph kernel network does have the above desired properties and show competitive performance compared to the stat of the art solvers.

1 INTRODUCTION

There are numerous applications in which it is desirable to learn a mapping between Banach spaces. In particular, either the input or the output space, or both, may be infinite dimensional. The possibility of learning such mappings opens up a new class of problems in the design of neural networks, with widespread potential applicability. New ideas are required to build on traditional neural networks which are mappings from finite dimensional Euclidean spaces into classes, or into another finite-dimensional Euclidean space. We study the development of neural networks in the setting in which the input and output spaces comprise real-valued functions defined on a bounded open set D in $\mathbb{R}^d$.

1.1 Literature Review And Context

We formulate a new class of neural networks, which are defined to map between spaces of functions on $\mathbb{R}^d$. Such neural networks, once trained, have the important property that they are discretization invariant, sharing the same network parameters between different discretizations. In contrast, standard neural network architectures depend heavily on the discretization and have difficulty in generalizing between different grid representations. Our methodology has an underlying Nyström approximation formulation [Nyström et al., 1930] which links different grids to a single set of network parameters. We illustrate the new conceptual class of neural networks within the context of partial differential equations, and the mapping between input data (in the form of a function) and output data (the function which solves the PDE). Both supervised and semisupervised settings are considered.

In PDE applications, the defining equations are often local, whilst the solution operator has non-local effects which, nonetheless, decay. Such non-local effects can be described by integral operators with graph approximations of Nyström type [Belongie et al., 2002] providing a consistent way of connecting different grid or data structures arising in computational methods. For this reason, graph networks hold great potential for the solution operators of PDEs, which is the departure for our work.

Partial Differential Equations (PDEs). A wide range of important engineering and physical problems are governed by PDEs. Over the past few decades, significant progress has been made on formulating [Gurtin, 1982] and solving [Johnson, 2012] the governing PDEs in many scientific fields from micro-scale problems (e.g., quantum and molecular dynamics) to macro-scale applications (e.g., civil and marine engineering). Despite the success in the application of PDEs to solve real-life problems, two significant challenges remain. First, identifying/formulating the underlying PDEs appropriate for the modeling of a specific problem usually requires extensive prior knowledge in the corresponding field which is then combined with universal conservation laws to design a predictive model; for example, modelling the deformation and fracture of solid structures requires detailed knowledge on the relationship between stress and strain in the constituent material. For complicated systems such as living cells, acquiring such knowledge is often elusive and formulating the governing PDE for these systems remains prohibitive; the possibility of learning such knowledge from data may revolutionize such fields. Second, solving complicated non-linear PDE systems (such as those arising in turbulence and plasticity) is computationally demanding; again the possibility of using instances of data from such computations to design fast approximate solvers holds great potential. In both these challenges, if neural networks are to play a role in exploiting the increasing volume of available data, then there is a need to formulate them so that they are well-adapted to mappings between function spaces.

We first outline two major neural network based approaches for PDEs. We consider PDEs of the form

$$\begin{aligned} (\mathcal{L}_a u)(x) &= f(x), \qquad && x \in D \\ u(x) &= 0, && x \in \partial D, \end{aligned} \tag{1}$$

with solution $u : D \to \mathbb{R}$, and parameter $a : D \to \mathbb{R}$ entering the defintion of $\mathcal{L}_a$. The domain D is discretized into K points (see Section 2) and N training pairs of coefficient functions and (approximate) solution functions $\{a_j, u_j\}_{j=1}^N$ are used to design a neural network. The first approach parametrizes the solution operator as a deep convolutional neural network between finite Euclidean space $\mathcal{F} : \mathbb{R}^K \times \Theta \to \mathbb{R}^K$ [Guo et al., 2016, Zhu and Zabaras, 2018, Adler and Oktem, 2017, Bhatnagar et al., 2019]. Such an approach is, by definition, not mesh independent and will need modifications to the architecture for different resolution and discretization of K in order to achieve consistent error (if at all possible). We demonstrate this issue in section 4 using the architecture of [Zhu and Zabaras, 2018] which was designed for the solution of (3) on a uniform 64×64 mesh. Furthermore this approach is limited to the discretization size and geometry of the training data hence it is not possible to query solutions at new points in the domain. We show both invariance of the error to resolution and our method's ability to transfer the solution between meshes in section 4.

The second approach directly parameterizes the solution u as a neural network $\mathcal{F} : D \times \Theta \to \mathbb{R}$ [E and Yu, 2018, Raissi et al., 2019, Bar and Sochen, 2019]. This approach is, of course, mesh independent since the solution is defined on the physical domain. However the parametric dependence is accounted for in a mesh-dependent fashion. Indeed, for any given new equation with new coefficient function a, one would need to train a new neural network $\mathcal{F}_a$. Such an approach closely resembles classical methods such as finite elements, replacing the linear span of a finite set of local basis with the space of neural networks. This approach suffers from the same computational issue as the classical methods: one needs to solve an optimization problem for every new parameter. Furthermore, the approach is limited to a setting in which the underlying PDE is known; purely data-driven learning of a map between spaces of functions is not possible.

Our methodology can be understood as a generalization of the above approaches. It most closely resembles the classical reduced basis method [DeVore, 2014] or the method of [Cohen and DeVore, 2015]. Our method, to the best of our knowledge, is the first practical deep learning method that is able to learn maps between infinite dimensional spaces. It remedies the mesh-dependent nature of the approach in [Guo et al., 2016, Zhu and Zabaras, 2018, Adler and Oktem, 2017, Bhatnagar et al., 2019] by producing a quality of approximation that is invariant to the resolution of the function and having the ability to transfer solutions between meshes. Moreover, it needs to only be trained once on the equations set $\{a_j, u_j\}_{j=1}^N$ and obtaining a solution for a new $a \sim \mu$ only requires a forward pass of the network, alleviating the major computational issues incurred in [E and Yu, 2018, Raissi et al., 2019, Herrmann et al., 2020, Bar and Sochen, 2019]. Lastly, our method requires no knowledge of the underlying PDE; the true map $\mathcal{F}^\dagger$ can be treated as a black-box, perhaps trained on experimental data or on the output of a costly computer simulation which is not necessarily a PDE.

Graph Neural Networks. Graph neural network (GNNs), a class of neural networks that apply on graph-structured data, have recently been developed and seen a variety of applications. Graph networks

Figure 1: Train On 16×16, Test On 241×241

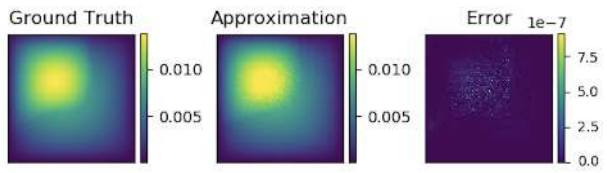

Graph kernel network is invariant of resolution. It can train on small resolution and generalize to large resolution, thereby avoid the large complexity scaling on grid size. Error is the squared l_2 absolute error on Darcy Equation.

incorporate an array of techniques such as graph convolution, edge convolution, attention, and graph pooling [Kipf and Welling, 2016, Hamilton et al., 2017, Gilmer et al., 2017, Veličković et al., 2017, Murphy et al., 2018]. GNNs have also been applied to the modeling of physical phenomena such as molecules [Chen et al., 2019] and rigid body systems [Battaglia et al., 2018], as these problems exhibit a natural graph interpretation: the particles are the nodes and the interactions are the edges.

The work [Alet et al., 2019] performed an initial study that employs graph networks on the problem of learning solutions to Poisson's equation among other physical applications. They propose an encoder-decoder setting, constructing graphs in the latent space and utilizing message passing between the encoder and decoder. However their model uses a nearest neighbor structure that is unable to capture non-local dependencies as the mesh size is increased. In contrast, we directly construct a graph in which the nodes are located on the spatial domain of the output function. Through message passing, we are then able to directly learn the kernel of the network which approximates the PDE solution. When querying a new location, we simply add a new node to our spatial graph and connect it to the existing nodes, avoiding interpolation error by leveraging the power of the Nyström extension for integral operators.

Continuous Neural Networks. The concept of defining neural networks in infinite-dimensional spaces is a central problem that long been studied [Williams, 1996, Neal, 1996, Roux and Bengio, 2007, Globerson and Livni, 2016, Guss, 2016]. The general idea is to take the infinite-width limit which yields a non-parametric method and has connections to Gaussian Process Regression [Neal, 1996, Matthews et al., 2018, Garriga-Alonso et al., 2018, Rasmussen and Williams, 2005]. Such methods have never been applied to PDE problems and have thus far not yielded efficient numerical algorithms that can parallel the success of convolutional or recurrent neural networks in finite dimensions. For an overview of non-parametric methods applied to PDE(s) see [Dunlop et al., 2018] and references therein. Another idea is to simply define a sequence of compositions where each layer is a map between infinite dimensional spaces with a finite-dimensional parametric dependence. This is the approach we take in this work, going a step further by sharing parameters between each layer.

1.2 Our Contributions

We introduce a new neural network architecture which is appropriate for the learning of mappings between spaces of functions defined on bounded open subsets of $\mathbb{R}^d$.

- Unlike existing methods, our approach is demonstrably able to share a single set of neural network parameters between methods based on different approximation methods and different grids, as demonstrated in Figure 1.
- A Nyström extension connects the neural network on function space to families of GNNs on arbitrary, possibly unstructured, grids.
- The method is demonstrated to have competitive approximation accuracy, as shown in the experiments.
- The ability of transfer learning between different discretizations with one set of parameters .
- The ability of semi-supervised learning that learns from data at a few points and the generalizes to the whole domain.

These concepts are illustrated in the context of a family of elliptic PDEs prototypical of a number of problems arising throughout the sciences and engineering.

2 PROBLEM SETTING

Our goal is to learn a mapping between two infinite dimensional spaces by using a finite collection of observations of input-output pairs from this mapping: supervised learning. Let $\mathcal{A}$ and $\mathcal{U}$ be separable Banach spaces and $\mathcal{F}^\dagger : \mathcal{A} \to \mathcal{U}$ a (typically) non-linear map. Suppose we have observations $\{a_j, u_j\}_{j=1}^N$ where $a_j \sim \mu$ is an i.i.d. sequence from the probability measure μ supported on $\mathcal{A}$ and $u_j = \mathcal{F}^\dagger(a_j)$ is possibly corrupted with noise. We aim to build an approximation of $\mathcal{F}^\dagger$ by constructing a parametric map

$$\mathcal{F} : \mathcal{A} \times \Theta \to \mathcal{U} \tag{2}$$

for some finite-dimensional parameter space Θ and then choosing $\theta^\dagger \in \Theta$ so that $\mathcal{F}(\cdot, \theta^\dagger) \approx \mathcal{F}^\dagger$.

This a natural framework for learning in infinite-dimensions as one could define a cost functional $C : \mathcal{U} \times \mathcal{U} \to \mathbb{R}$ and seek a minimizer of the problem

$$\min_{\theta \in \Theta} \mathbb{E}_{a \sim \mu}[C(\mathcal{F}(a, \theta), \mathcal{F}^\dagger(a))]$$

which directly parallels the classical finite-dimensional setting [Vapnik, 1998]. Showing the existence of minimizers, in the infinite-dimensional setting, remains a challenging open problem. We will approach this problem in the test-train setting in which empirical approximations to the cost are used. We conceptualize our methodology in the infinite-dimensional setting. This means that all finite-dimensional approximations can share a common set of network parameters which are defined in the (approximation-free) infinite-dimensional setting. To be concrete we will consider infinite-dimensional spaces which are Banach spaces of real-valued functions defined on a bounded open set in $\mathbb{R}^d$. We then consider mappings $\mathcal{F}^\dagger$ which take input functions to a PDE and map them to solutions of the PDE, both input and solutions being real-valued functions on $\mathbb{R}^d$.

A common instantiation of the preceding problem is the approximation of the second order elliptic PDE

$$\begin{aligned} -\nabla \cdot (a(x) \nabla u(x)) &= f(x), \quad & x \in D \\ u(x) &= 0, \quad & x \in \partial D \end{aligned} \tag{3}$$

for some bounded, open set $D \subset \mathbb{R}^d$ and a fixed function $f \in L^2(D; \mathbb{R})$. This equation is prototypical of PDEs arising in numerous applications including hydrology [Bear and Corapcioglu, 2012] and elasticity [Antman, 2005]. For a given $a \in \mathcal{A} = L^\infty(D; \mathbb{R}^+) \cap L^2(D; \mathbb{R}^+)$, equation (3) has a unique weak solution $u \in \mathcal{U} = H_0^1(D; \mathbb{R})$ [Evans, 2010] and therefore we can define the solution operator $\mathcal{F}^\dagger$ as the map $a \mapsto u$. Note that while the PDE (3) is linear, the solution operator $\mathcal{F}^\dagger$ is not.

Since our data a_j and u_j are , in general, functions, to work with them numerically, we assume access only to point-wise evaluations. To illustrate this, we will continue with the example of the preceding paragraph. To this end let $P_K = \{x_1, \dots, x_K\} \subset D$ be a K-point discretization of the domain D and assume we have observations $a_j|_{P_K}, u_j|_{P_K} \in \mathbb{R}^K$, for a finite collection of input-output pairs indexed by j. In the next section, we propose a kernel inspired graph neural network architecture which, while trained on the discretized data, can produce an answer $u(x)$ for any $x \in D$ given a new input $a \sim \mu$. That is to say that our approach is independent of the discretization P_K and therefore a true function space method; we verify this claim numerically by showing invariance of the error as $K \to \infty$. Such a property is highly desirable as it allows a transfer of solutions between different grid geometries and discretization sizes.

We note that, while the application of our methodology is based on having point-wise evaluations of the function, it is not limited by it. One may, for example, represent a function numerically as a finite set of truncated basis coefficients. Invariance of the representation would then be with respect to the size of this set. Our methodology can, in principle, be modified to accommodate this scenario through a suitably chosen architecture. We do not pursue this direction in the current work.

3 GRAPH KERNEL NETWORK

We propose a graph kernel neural network for the solution of the problem outlined in section 2. As a guiding principle of our architecture, we take the following example. Let $\mathcal{L}_a$ be a differential operator depending on a parameter $a \in \mathcal{A}$ and consider the PDE

$$\begin{aligned} (\mathcal{L}_a u)(x) &= f(x), \quad & x \in D \\ u(x) &= 0, \quad & x \in \partial D \end{aligned} \tag{4}$$

for a bounded, open set $D \subset \mathbb{R}^d$ and some fixed function f living in an appropriate function space determined by the structure of $\mathcal{L}_a$. The elliptic operator $\mathcal{L}_a \cdot = -\text{div}(a \nabla \cdot)$ from equation (3) is an example. Under fairly general conditions on $\mathcal{L}_a$ [Evans, 2010], we may define the Green's function $G : D \times D \to \mathbb{R}$ as the unique solution to the problem

$$\mathcal{L}_a G(x, \cdot) = \delta_x$$

where δ_x is the delta measure on $\mathbb{R}^d$ centered at x. Note that G will depend on the parameter a thus we will henceforth denote it as G_a. The solution to (4) can then be represented as

$$u(x) = \int_D G_a(x, y) f(y) \, dy. \tag{5}$$

Generally the Green's function is continuous at points $x \neq y$, for example, when $\mathcal{L}_a$ is uniformly elliptic [Gilbarg and Trudinger, 2015], hence it is natural to model it via a neural network. Guided by the representation (5), we propose the following iterative architecture for $t = 0, \dots, T - 1$.

$$\begin{aligned} v_{t+1}(x) = & \sigma\Big(W v_t(x) \\ & + \int_D \kappa_\phi(x, y, a(x), a(y)) v_t(y) \, \nu_x(dy) \Big) \end{aligned} \tag{6}$$

where $\sigma : \mathbb{R} \to \mathbb{R}$ is a fixed function applied elementwise, ν_x is a fixed Borel measure for each $x \in D$ and $W \in \mathbb{R}^{n \times n}$, together with the parameters ϕ entering kernel $\kappa_\phi : \mathbb{R}^{2(d+1)} \to \mathbb{R}^{n \times n}$, are to be learned from data. We model κ_ϕ as a neural network mapping $\mathbb{R}^{2(d+1)}$ to $\mathbb{R}^{n \times n}$.

Discretization of the continuum picture may be viewed as replacing Borel measure ν_x by an empirical approximation based on the K grid points being used. In this setting we may view κ_ϕ as a $K \times K$ kernel block matrix, where each entry $\kappa_\phi(x, y)$ is itself a $n \times n$ matrix. Each block shares the same set of network parameters. This is the key to making a method which shares common parameters independent of the discretization used.

Finally we observe that, although we have focussed on neural networks mapping a to u, generalizations are possible, such as mapping f to u, or having non-zero boundary data g on ∂D and mapping g to u. More generally one can consider the mapping from (a, f, g) into u and use similar ideas. To illustrate ideas we will consider the mapping from f to u below (which is linear and for which an analytic solution is known) before moving on study the (nonlinear) mapping from a to u. Since in the setting f is fixed, our iterative kernel integration convoluted with representation v instead of f.

Example: Poisson Equation. We consider a simplification of the foregoing in which we study the map from f to u. To this end we set $v_0(x) = f(x)$, $T = 1$, $n = 1$, $\sigma(x) = x$, $W = w = 0$, and $\nu_x(dy) = dy$ (the Lebesgue measure) in (6). We then obtain the representation (5) with the Green's function G_a parameterized by the neural network κ_ϕ with explicit dependence on $a(x)$, $a(y)$. Now consider the setting where $D = [0, 1]$ and $a(x) \equiv 1$, so that (3) reduces to the 1-dimensional Poisson equation with explicitly computable Green's function. Indeed,

$$G(x, y) = \frac{1}{2}\left(x + y - |y - x|\right) - xy.$$

Note that although the map $f \mapsto u$ is, in function space, linear, the Green's function itself is not linear in either argument. Figure 2 shows κ_ϕ after training with $N = 2048$ samples $f_j \sim \mu = \mathcal{N}(0, (-\Delta + I)^{-1})$ with periodic boundary conditions on the operator $-\Delta + I$. Notice that we are able to almost perfectly capture the geometry of the Green's function. The learned solution map is universal: once we have this approximation of the Green's function we can map *any* $f \in L^2(D; \mathbb{R})$ into solution $u \in L^2(D; \mathbb{R})$, even though though the training was entirely from data drawn from μ. While the approximation is not perfect, this result is quite remarkable and speaks to the generalization capabilities of our overall approach. Furthermore, the training data f_j, u_j are specified on an 85-point uniform discretization of D while κ_ϕ is evaluated on a 256×256 uniform grid, demonstrating our method's mesh invariance property.

Algorithmic Framework. The initialization $v_0(x)$ to our network (6) can be viewed as the initial guess we make for the solution $u(x)$ as well as any other dependence we want to make explicit. A natural choice is to start with the coefficient $a(x)$ itself as well as the position in physical space x. This $(d+1)$-dimensional vector field is then lifted to a n-dimensional vector field, an operation which we may view as the first layer of the overarching neural network. This is then used as an initialization to the kernel neural network, which is iterated T times. In the final layer, we project back to the scalar field of interest with another neural network layer.

Due to the smoothing effect of the inverse elliptic operator in (3) with respect to the input data a (and indeed f when we consider this as input), we augment the initialization $(x, a(x))$ with a Gaussian smoothed version of the coefficients $a_\epsilon(x)$, together with their gradient $\nabla a_\epsilon(x)$. Thus we initialize with a $2(d + 1)$-dimensional vector field. Throughout this paper the Gaussian smoothing is performed with a centred isotropic Gaussian with variance 5. The Borel measure ν_x is chosen to be the Lebesgue measure supported on a ball at x of radius r. Thus we have

$$v_0(x) = P(x, a(x), a_\epsilon(x), \nabla a_\epsilon(x)) + p \tag{7}$$

$$v_{t+1}(x) = \sigma\Big(W v_t(x) + \int_{B(x,r)} \kappa_\phi\big(x, y, a(x), a(y)\big) v_t(y)\, \mathrm{d}y\Big) \tag{8}$$

$$u(x) = Q v_T(x) + q \tag{9}$$

where $P \in \mathbb{R}^{n \times 2(d+1)}$, $p \in \mathbb{R}^n$, $v_t(x) \in \mathbb{R}^n$ and $Q \in \mathbb{R}^{1 \times n}$, $q \in \mathbb{R}$. The integration in (8) is approximated by a Monte Carlo sum via a message passing graph network with edge weights $(x, y, a(x), a(y))$. The choice of measure $\nu_x(\mathrm{d}y) = \mathbb{1}_{B(x,r)}\mathrm{d}y$ is two-fold: 1) it allows for more efficient computation and 2) it exploits the decay property of the Green's function. Note that if more information is known about the true kernel, it can be added into this measure. For example, if we know the true kernel has a Gaussian structure, we can define $\nu_x(\mathrm{d}y) = \mathbb{1}_{B(x,r)}\rho_x(y)\mathrm{d}y$ where $\rho_x(y)$ is a Gaussian density. Then κ_ϕ will need to learn a much less complicated function. We however do not pursue this direction in the current line of work.

Message Passing Graph Networks. Message passing graph networks comprise a standard architecture em-

Figure 2: Kernel For One-Dimensional Green's Function

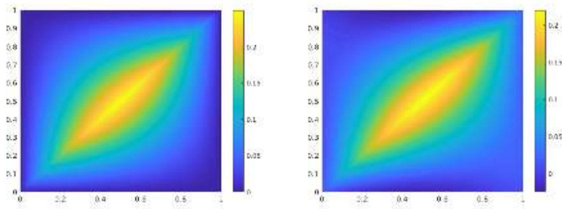

Proof of concept: graph kernel network on 1 dimensional Poisson equation; comparison of learned and truth kernel.

ploying edge features [Gilmer et al., 2017]. If we properly construct the graph on the spatial domain D of the PDE, the kernel integration can be viewed as an aggregations of messages. Given node features $v_t(x) \in \mathbb{R}^n$, edge features $e(x,y) \in \mathbb{R}^{n_e}$, and a graph G, the message passing neural network with averaging aggregation is

$$v_{t+1}(x) = Wv_t(x) + \frac{1}{|N(x)|} \sum_{y \in N(x)} \kappa_\phi\big(e(x,y)\big) v_t(y) \tag{10}$$

where $W \in \mathbb{R}^{n \times n}$, $N(x)$ is the neighborhood of x according to the graph, $\kappa_\phi\big(e(x,y)\big)$ is a neural network taking as input edge features and as output a matrix in $\mathbb{R}^{n \times n}$. In relation to (8), $e(x,y) = (x, y, a(x), a(y)) \in \mathbb{R}^{2(d+1)}$.

Graph Construction. To use the message passing framework (10), we need to design a graph which connects the physical domain D of the PDE. The nodes are chosen to be the K discretized spatial locations. Here we work on a standard uniform mesh, but there are many other possibilities such as finite-element triangulations. The edge connectivity is then chosen according to the integration measure in (8). In particular, each node $x \in \mathbb{R}^d$ is connected to all neighboring nodes which lie within the ball $B(x,r)$, defining the neighborhood set $N(x)$. Then for each neighbor $y \in N(x)$, we assign the edge weight $e(x,y) = (x, y, a(x), a(y))$. Equation (10) can then be viewed as a Monte Carlo approximation of (8). This local structure allows for more efficient computation while remaining invariant to mesh-refinement. Indeed, since the radius parameter r is chosen in physical space, the size of the set $N(x)$ grows as the disretization size K grows. This is a key feature which makes our methodology mesh-independent.

Nyström Approximation of the Kernel. While the aforementioned graph structure severely reduces the computational overhead of integrating over the entire domain D (corresponding to a fully-connected graph), the number of edges still scale like $\mathcal{O}(K^2)$. To overcome this, we employ a random Nyström-type approximation of the kernel. In particular, we uniformly sample $m \ll K$ nodes from the original graph, constructing a new random sub-graph. This process is repeated $l \in \mathbb{N}$ times, yielding l random sub-graphs each with m nodes. This can be thought of as a way of reducing the variance in the estimator. We use these subgraphs when evaluating (10) during training which gives the more favorable scaling $\mathcal{O}(lm^2)$. Indeed, numerically we find that $l = 4$ and $m = 200$ is sufficient even when $K = 421^2 = 177,241$. In the evaluation phase, when we want the solution on a particular mesh geometry, we simply partition the mesh into sub-graphs each with m nodes and evaluate each separately.

We will now demonstrate the quality of this kernel approximation in a RHKS setting. A real Reproducing Kernel Hilbert Space (RKHS) $(\mathcal{H}, \langle\cdot,\cdot\rangle, \|\cdot\|)$ is a Hilbert space of functions $f : D \to \mathbb{R}$ where point-wise evaluation is a continuous linear functional, i.e. $|f(x)| \leq C\|f\|$ for some constant $C \geq 0$, independent of x. For every RHKS, there exists a unique, symmetric, positive definite kernel $\kappa : D \times D \to \mathbb{R}$, which gives the representation $f(x) = \langle f, \kappa(\cdot, x)\rangle$. Let $T : \mathcal{H} \to \mathcal{H}$ be a linear operator on $\mathcal{H}$ acting via the kernel

$$Tf = \int_{B(\cdot,r)} \kappa(\cdot, y) f(y) \nu(dy).$$

Let $T_m : \mathcal{H} \to \mathcal{H}$ be its m-point empirical approximation

$$T_m = \int_{B(\cdot,r)} \kappa(\cdot, y) f(y) \nu_m(dy)$$

hence

$$\nu_m(dy) = \frac{1}{m} \sum_{k=1}^{m} \delta_{y_k}(dy),$$

$$T_m f = \frac{1}{m} \sum_{k=1}^{m} \kappa(\cdot, y_k) f(y_k).$$

The error of this approximation achieves the Monte Carlo rate $O(m^{-1/2})$:

Proposition 1. *Suppose* $\mathbb{E}_{y \sim \nu}[\kappa(\cdot, y)^4] < \infty$ *then there exists a constant* $C \geq 0$ *such that*

$$\mathbb{E}\|T - T_m\|_{HS} \leq \frac{C}{\sqrt{m}}$$

where $\|\cdot\|_{HS}$ *denotes the Hilbert-Schmidt norm on operators acting on* $\mathcal{H}$*.*

For a proof of this result see Appendix A.1. Assuming boundedness of the kernel κ, one can prove similar results that, instead of in expectation, hold with high probability [Rosasco et al., 2010].

We note that, in our algorithm, $\kappa : D \times D \to \mathbb{R}^{n \times n}$ whereas the preceding results are proven only in the setting $n = 1$; nonetheless they provide useful intuition regarding the approximations used in our methodology.

4 EXPERIMENTS

In this section we demonstrate that the claimed properties of our methodology and compare to existing approaches in the literature. All experimental results concern the mapping $a \mapsto u$ defined by (3) with $D = [0, 1]^2$. Coefficients are generated according to $a \sim \psi_{\#}\mu$ where $\mu = \mathcal{N}(0, (-\Delta + 9I)^{-3})$ with a Neumann boundry condition on the operator $-\Delta + 9I$. The mapping $\psi : \mathbb{R} \to \mathbb{R}$ takes the value 12 on the positive part of the real line and 3 on the negative hence the coefficients are piece-wise constant with a random geometry and a fixed contrast of 4. Such constructions are common in the modeling of material microstructures and sub-surface flows. Solutions u are obtained by using a second-order finite difference scheme on a 241×241 grid. Different resolutions are downsampled from this dataset.

Without special notice we set the dimension of representation n (i.e. the width of graph network) to be 64, the number of iteration T to be 6, σ to be ReLU, and the inner kernel network κ to be a 3 layers feed-forward network with widths $(6, 512, 1024, n^2)$ and ReLU activation. We use Adam optimizer with the learning rate $1e-4$ and train for 200 epochs, unless otherwise stated. These hyperparameters are not optimized and should be free to change in practice. We adapt the message passing network from the standard Pytorch graph network library Torch-geometric [Fey and Lenssen, 2019]. All errors are relative L^2 errors.

4.1 Supervised Setting

First we consider the supervised scenario that we are given N training pairs $\{a_j, u_j\}_1^N$, where each a_j and u_j are provided on a $s \times s$ grid ($K = s^2$).

Generalization of Resolutions on Full Grids. To examine the generalization property, we train the graph kernel network on resolution $s \times s$ and test on another resolution $s' \times s'$. We fix the radius to be $r = 0.10$, train on $N = 100$ equation pairs and test on 40 equation pairs.

Table 1: Comparing Resolutions On Full Grids

Resolutions	$s' = 16$	$s' = 31$	$s' = 61$
$s = 16$	0.0525	0.0591	0.0585
$s = 31$	0.0787	0.0538	0.0588

$r = 0.10$, $N = 100$, relative l_2 test error

As shown in Table 1, for each row, the test errors of different resolutions remain on the same scale, which means graph kernel networks can train on one resolution and generalize to another resolution. The test errors on the diagonal ($s = s' = 16$ and $s = s' = 31$) are the smallest, which means the network has the best performance when the training grid and the test grid are the same. Interestingly, for the second row, when training on $s = 31$, it is easier to general to $s' = 61$ than to $s' = 16$. This is because when generalizing to a larger grid, the support of the kernel becomes large which does not hurt the performance. But when generalizing to a smaller grid, part of the support of the kernel is lost, which causes the kernel to be inaccurate.

Expressiveness and Overfitting We compare the training error and test error with a different number of training pairs N to see if the kernel network can learn the kernel structure even with a small amount of data. We study the expressiveness of kernel network, examining how it overfits. We fix $r = 0.10$ on the $s = s' = 31$ grid and train with $N = 10, 100, 1000$ and 5000, 500, 100 epochs respectively.

Table 2: Comparing Number of Training Pairs

Training Size	**Training Error**	**Test Error**
$N = 10$	0.0111	0.0876
$N = 100$	0.0056	0.0455
$N = 1000$	0.0073	0.0307

5000, 500, 100 epochs respectively.

We see from Table 2 that the kernel network already achieves a reasonable result when $N = 10$, and the accuracy is competitive when $N = 100$. In all three cases, the test error is larger than the training error which means the kernel network has enough expressiveness to overfit the training set. Thos overfitting is not severe as the training error will not be pushed to zero even for $N = 10$, after 5000 epochs.

4.2 Semi-Supervised Setting

In the semi-supervised setting, we are only given m nodes sampled from a $s \times s$ grid for each training pair, and want to evaluate on m' nodes sampled from a $s' \times s'$ grid for each test pair. Without special notice, we set the number of sampled nodes $m = m' = 200$. For each training pair, we sample twice $l = 2$; for each test pair, we sample once $l' = 1$. We train on $N = 100$ equations and test on $N' = 100$ equations. The radius for both training and testing is set to $r = r' = 0.25$.

Generalization of Resolutions on Sampled Grids. Similar to the first experiments, we train the graph kernel network with nodes sampled from the $s \times s$ resolution and test on nodes sampled from the $s' \times s'$ resolution.

Table 3: Generalization of Resolutions on Sampled Grids

Resolutions	$s' = 61$	$s' = 121$	$s' = 241$
$s = 16$	0.0717	0.0768	0.0724
$s = 31$	0.0726	0.0710	0.0722
$s = 61$	0.0687	0.0728	0.0723
$s = 121$	0.0687	0.0664	0.0685
$s = 241$	0.0649	0.0658	0.0649

$N = 100, m = m' = 200, r = r' = 0.25, l = 2$

As shown in Table 3, for each row, the test errors on different resolutions are about the same, which means the graph kernel network can also generalize in the semi-supervised setting. Comparing the rows, large training resolutions s tend to have a smaller error. When sampled from a finer grid, there are more variety of edges i.e. the support of the kernel is larger on the finer grid. Still, the performance is best when $s = s'$.

The Number of Examples v.s. the Times of Sampling. Increasing the number of times we sample l, will reduce the error from Nyström approximation. By comparing different l we want to find which number will be sufficient. When we sample l times for each equation, we will get Nl number of sampled training pairs. We are also interested in fixing the total number of sample training pairs; for example, how will $N = 100, l = 10$ compare to $N = 1000, l = 1$.

Table 4: The Number of Training Equations and the Number of Sampling

	$l = 1$	$l = 2$	$l = 4$	$l = 8$
$N = 10$	0.1259	0.1069	0.0967	0.1026
$N = 100$	0.0786	0.0687	0.0690	0.0621
$N = 1000$	0.0604	0.0579	0.0540	0.0483

$s = 121, m = m' = 200, r = r' = 0.25$

As shown in Table 4, in general the larger l the better, but $l = 2$ already gives good results. Meanwhile, $(N = 100, l = 8)$ has near the same error as $(N = 1000, l = 1)$, which implies we can increasing l when the amount of training data is small.

Different Number of Nodes in Training and Testing. To further examine the Nyström approximation, we compare different numbers of node samples m, m' for both training and testing.

Table 5: Comparing the Number of Nodes in the Training and Testing

$m' =$	100	200	400	800
$m = 100$	0.0871	0.0716	0.0662	0.0609
$m = 200$	0.0972	0.0734	0.0606	0.0562
$m = 400$	0.0991	0.0699	0.0560	0.0506
$m = 800$	0.1084	0.0751	0.0573	0.0478

$s = 121, r = r' = 0.15, l = 5$

As can be seen from Table 5, in general the large m and m' the better. For each row, fixing m, the larger m' the better. But for each column, when fixing m', increasing m may not lead to better performance. This is again due to the fact that when learning on a larger grid, the kernel network learns a kernel with larger support. When evaluating on a smaller grid, the learned kernel will be truncated to have small support which grows the error. In general, $m = m'$ will be the best choice.

The Number of Nodes and the Radius. The computation and storage of graph networks directly scale with the number of edges. In this experiment we want to study the trade off between the number of nodes m and the radius r when fixing the number of edges.

Table 6: The Number of Nodes and the Radius

r	m	**Edges**	**Error**
0.05	100	176	0.1108
0.05	200	666	0.1090
0.05	400	3354	0.0994
0.15	100	512	0.0860
0.15	200	2770	0.0705
0.15	400	14086	0.0539
0.40	100	1596	0.0649
0.40	200	9728	0.0517
0.40	400	55919	0.0407

$s = 121, l = 5, m' = m$

As shown in Table 6, the more edges the better. But when fixing the number of edges, the performance depends more on the radius r than on the number of nodes m. In other words, the error of truncating the kernel locally is larger than the error from Nyström approximation. It would be better to use larger r with smaller m.

4.3 Full Scale Comparison with Different Benchmarks

In the following section, we compare kernel networks with different benchmarks. The network is trained and evaluated on the same full grid. The results are presented in Table 7. **NN** is a simple point-wise feed-forward neural network. It is mesh-free, but perform badly due to lack of neighbor information. **FCN** is the state of the art neural network method based on Fully Convolution Network [Zhu and Zabaras, 2018]. It has a dominating performance for small grids $s = 61$. But fully convolution networks are mesh-dependent and therefore their error grows when moving to a larger grid. **PCA+NN** is an instantiation of the methodology proposed in [Bhattacharya et al., 2020]: using PCA as an autoencoder on both the input and output data and interpolating the latent spaces with a neural network. The method provably obtains mesh-independent error and can learn purely from data, however the solution can only be evaluated on the same mesh as the training data. **RBM** is the classical Reduced Basis Method (using a PCA basis), which is widely used in application and provably obtains mesh-independent error [DeVore, 2014]. It has the best performance but the solutions can only be evaluated on the same mesh as the training data and one needs knowledge of the PDE to employ it. **KernelGNN** stands for our graph kernel network. It enjoys competitive performance against all other methods while being able to generalize to different mesh geometries. Some figures of KernelGNN are included in Appendix A.2.

Table 7: Scaling of different network architectures

Networks	141	211	421
NN	0.1716	0.1716	0.1716
FCN	0.0493	0.0727	0.1097
PCA+NN	0.0298	0.0298	0.0299
RBM	0.0251	0.0255	0.0259
KernelGNN	0.0332	0.0342	0.0369

5 DISCUSSION AND FUTURE WORK

As shown in the experiments, we can conclude graph kernel networks do have the desired mesh-free property. It can learn the infinite-dimension mapping between functions space, instead of a mapping between fixed discretization. Meanwhile, it can achieve competitive performance compared to those mesh dependent solver. Such a mesh-free method has many applications. It has the potential to be a faster solver that learns from only a few points and a few equations. It is the only method that can works in the semi-supervised scenario, when we only have measurements on some parts of the grid. It is also the only method that can transfer between different geometry. For example, when computing the flow dynamic of many different airfoils, we can construct different graphs and train together. When learning from irregular grids and querying new locations, our method does not require any interpolation, avoid subsequently interpolation error.

Disadvantage. Graph kernel network's runtime and storage scale with the number of edges $E = O(K^2)$. While other mesh-dependent methods such as PCA+NN and RBF require only $O(K)$. This is somewhat inevitable, because to learn the continuous function or the kernel, we need to capture pairwise information between every two nodes, which is $O(K)$, whereas when the discretization is fixed, one just need to capture the point-wise information, which is $O(K)$. Therefore training and evaluating the whole grid is costly when the grid is large. On the other hand, doing sampling loses some information about the data, which causes an error and makes our method not as good as PCA+NN and RBM.

Future Work. To deal with the above problem, we purpose a more efficient way to make use of the full grid – multi-grid method. Instead of doing sampling and throw most of the nodes away, we can construct multi graphs corresponding to different resolutions, so that within each graph, nodes only connect to their nearest neighbors. The number of edges then scale as $O(K)$ instead of $O(K^2)$. The error term from Nyström approximation can be avoided.

Another direction is to extend the framework for time-dependent PDEs. Since the graph kernel network is itself an iterative solver with the time step t, it is natural to frame it as an RNN that each time step corresponds to a time step of the PDEs.

References

[Adler and Oktem, 2017] Adler, J. and Oktem, O. (2017). Solving ill-posed inverse problems using iterative deep neural networks. *Inverse Problems*.

[Alet et al., 2019] Alet, F., Jeewajee, A. K., Villalonga, M. B., Rodriguez, A., Lozano-Perez, T., and Kaelbling, L. (2019). Graph element networks: adaptive, structured computation and memory. In *36th International Conference on Machine Learning*. PMLR.

[Antman, 2005] Antman, S. S. (2005). *Problems In Nonlinear Elasticity*. Springer.

[Bar and Sochen, 2019] Bar, L. and Sochen, N. (2019). Unsupervised deep learning algorithm for pde-based forward and inverse problems. *arXiv preprint arXiv:1904.05417*.

[Battaglia et al., 2018] Battaglia, P. W., Hamrick, J. B., Bapst, V., Sanchez-Gonzalez, A., Zambaldi, V., Malinowski, M., Tacchetti, A., Raposo, D., Santoro, A., Faulkner, R., et al. (2018). Relational inductive biases, deep learning, and graph networks. *arXiv preprint arXiv:1806.01261*.

[Bear and Corapcioglu, 2012] Bear, J. and Corapcioglu, M. Y. (2012). *Fundamentals of transport phenomena in porous media*, volume 82. Springer Science & Business Media.

[Belongie et al., 2002] Belongie, S., Fowlkes, C., Chung, F., and Malik, J. (2002). Spectral partitioning with indefinite kernels using the nyström extension. In *European conference on computer vision*, pages 531–542. Springer.

[Bhatnagar et al., 2019] Bhatnagar, S., Afshar, Y., Pan, S., Duraisamy, K., and Kaushik, S. (2019). Prediction of aerodynamic flow fields using convolutional neural networks. *Computational Mechanics*, pages 1–21.

[Bhattacharya et al., 2020] Bhattacharya, K., Kovachki, N. B., and Stuart, A. M. (2020). Model reduction and neural networks for parametric pde(s). *preprint*.

[Chen et al., 2019] Chen, C., Ye, W., Zuo, Y., Zheng, C., and Ong, S. P. (2019). Graph networks as a universal machine learning framework for molecules and crystals. *Chemistry of Materials*, 31(9):3564–3572.

[Cohen and DeVore, 2015] Cohen, A. and DeVore, R. (2015). Approximation of high-dimensional parametric pdes. *Acta Numerica*, page 1159.

[DeVore, 2014] DeVore, R. A. (2014). *Chapter 3: The Theoretical Foundation of Reduced Basis Methods*.

[Dunlop et al., 2018] Dunlop, M. M., Girolami, M. A., Stuart, A. M., and Teckentrup, A. L. (2018). How deep are deep gaussian processes? *The Journal of Machine Learning Research*, 19(1):2100–2145.

[E and Yu, 2018] E, W. and Yu, B. (2018). The deep ritz method: A deep learning-based numerical algorithm for solving variational problems. *Communications in Mathematics and Statistics*, 6(1).

[Evans, 2010] Evans, L. C. (2010). *Partial Differential Equations*, volume 19. American Mathematical Soc.

[Fey and Lenssen, 2019] Fey, M. and Lenssen, J. E. (2019). Fast graph representation learning with PyTorch Geometric. In *ICLR Workshop on Representation Learning on Graphs and Manifolds*.

[Garriga-Alonso et al., 2018] Garriga-Alonso, A., Rasmussen, C. E., and Aitchison, L. (2018). Deep Convolutional Networks as shallow Gaussian Processes. *arXiv e-prints*, page arXiv:1808.05587.

[Gilbarg and Trudinger, 2015] Gilbarg, D. and Trudinger, N. S. (2015). *Elliptic partial differential equations of second order*. springer.

[Gilmer et al., 2017] Gilmer, J., Schoenholz, S. S., Riley, P. F., Vinyals, O., and Dahl, G. E. (2017). Neural message passing for quantum chemistry. In *Proceedings of the 34th International Conference on Machine Learning-Volume 70*, pages 1263–1272. JMLR. org.

[Globerson and Livni, 2016] Globerson, A. and Livni, R. (2016). Learning infinite-layer networks: Beyond the kernel trick. *CoRR*, abs/1606.05316.

[Guo et al., 2016] Guo, X., Li, W., and Iorio, F. (2016). Convolutional neural networks for steady flow approximation. In *Proceedings of the 22nd ACM SIGKDD International Conference on Knowledge Discovery and Data Mining*, pages 481–490. ACM.

[Gurtin, 1982] Gurtin, M. E. (1982). *An introduction to continuum mechanics*. Academic press.

[Guss, 2016] Guss, W. H. (2016). Deep Function Machines: Generalized Neural Networks for Topological Layer Expression. *arXiv e-prints*, page arXiv:1612.04799.

[Hamilton et al., 2017] Hamilton, W., Ying, Z., and Leskovec, J. (2017). Inductive representation learning on large graphs. In *Advances in neural information processing systems*, pages 1024–1034.

[Herrmann et al., 2020] Herrmann, L., Schwab, C., and Zech, J. (2020). Deep relu neural network expression rates for data-to-qoi maps in bayesian pde inversion.

[Johnson, 2012] Johnson, C. (2012). *Numerical solution of partial differential equations by the finite element method*. Courier Corporation.

[Kipf and Welling, 2016] Kipf, T. N. and Welling, M. (2016). Semi-supervised classification with graph convolutional networks. *arXiv preprint arXiv:1609.02907*.

[Matthews et al., 2018] Matthews, A. G. d. G., Rowland, M., Hron, J., Turner, R. E., and Ghahramani, Z. (2018). Gaussian Process Behaviour in Wide Deep Neural Networks. *arXiv e-prints*, page arXiv:1804.11271.

[Murphy et al., 2018] Murphy, R. L., Srinivasan, B., Rao, V., and Ribeiro, B. (2018). Janossy pooling: Learning deep permutation-invariant functions for variable-size inputs. *arXiv preprint arXiv:1811.01900*.

[Neal, 1996] Neal, R. M. (1996). *Bayesian Learning for Neural Networks*. Springer-Verlag, Berlin, Heidelberg.

[Nyström et al., 1930] Nyström, E. J. et al. (1930). Über die praktische auflösung von integralgleichungen mit anwendungen auf randwertaufgaben. *Acta Mathematica*, 54.

[Raissi et al., 2019] Raissi, M., Perdikaris, P., and Karniadakis, G. E. (2019). Physics-informed neural networks: A deep learning framework for solving forward and inverse problems involving nonlinear partial differential equations. *Journal of Computational Physics*, 378:686–707.

[Rasmussen and Williams, 2005] Rasmussen, C. E. and Williams, C. K. I. (2005). *Gaussian Processes for Machine Learning (Adaptive Computation and Machine Learning)*. The MIT Press.

[Rosasco et al., 2010] Rosasco, L., Belkin, M., and Vito, E. D. (2010). On learning with integral operators. *J. Mach. Learn. Res.*, 11:905934.

[Roux and Bengio, 2007] Roux, N. L. and Bengio, Y. (2007). Continuous neural networks. In Meila, M. and Shen, X., editors, *Proceedings of the Eleventh International Conference on Artificial Intelligence and Statistics*, volume 2 of *Proceedings of Machine Learning Research*, pages 404–411, San Juan, Puerto Rico. PMLR.

[Vapnik, 1998] Vapnik, V. N. (1998). *Statistical Learning Theory*. Wiley-Interscience.

[Veličković et al., 2017] Veličković, P., Cucurull, G., Casanova, A., Romero, A., Lio, P., and Bengio, Y. (2017). Graph attention networks. *arXiv preprint arXiv:1710.10903*.

[Williams, 1996] Williams, C. K. I. (1996). Computing with infinite networks. In *Proceedings of the 9th International Conference on Neural Information Processing Systems*, NIPS96, page 295301, Cambridge, MA, USA. MIT Press.

[Zhu and Zabaras, 2018] Zhu, Y. and Zabaras, N. (2018). Bayesian deep convolutional encoderdecoder networks for surrogate modeling and uncertainty quantification. *Journal of Computational Physics*, 366:415 – 447.

A Appendix

A.1 Proof of Proposition 1

Proposition 1. Let $\{y_j\}_{j=1}^m$ be an i.i.d. sequence with $y_j \sim \nu$. Define $\kappa_y = \kappa(\cdot, y)$ for any $y \in D$. Notice that by the reproducing property,

$$\begin{aligned}\mathbb{E}_{y\sim\nu}[\mathbb{1}_{B(\cdot,r)}(\kappa_y \otimes \kappa_y)f] &= \mathbb{E}_{y\sim\nu}[\mathbb{1}_{B(\cdot,r)}\langle \kappa_y, f\rangle \kappa_y] \\ &= \int_D \mathbb{1}_{B(\cdot,r)}\langle \kappa_y, f\rangle \kappa_y \, \nu(dy) \\ &= \int_D \mathbb{1}_{B(\cdot,r)}\kappa(\cdot, y) f(y) \, \nu(dy) \\ &= \int_{B(\cdot,r)} \kappa(\cdot, y) f(y) \, \nu(dy)\end{aligned}$$

hence

$$T = \mathbb{E}_{y\sim\nu}[\mathbb{1}_{B(\cdot,r)}(\kappa_y \otimes \kappa_y)]$$

and similarly

$$T_m = \frac{1}{m}\sum_{j=1}^m \mathbb{1}(y_j \in B(\cdot, r))(\kappa_{y_j} \otimes \kappa_{y_j}).$$

Define $T^{(j)} := \mathbb{1}(y_j \in B(\cdot, r))(\kappa_{y_j} \otimes \kappa_{y_j})$ for any $j \in \{1, \dots, m\}$ and $T_y := \mathbb{1}_{B(\cdot,r)}(\kappa_y \otimes \kappa_y)$ for any $y \in D$, noting that $\mathbb{E}_{y\sim\nu}[T_y] = T$ and $\mathbb{E}[T^{(j)}] = T$. Further we note that

$$\mathbb{E}_{u\sim\nu}\|T_y\|_{HS}^2 \leq \mathbb{E}_{y\sim\nu}\|\kappa_y\|^4 < \infty$$

and, by Jensen's inequality,

$$\|T\|_{HS}^2 \leq \mathbb{E}_{y\sim\nu}\|T_y\|_{HS}^2 < \infty$$

hence T is Hilbert-Schmidt (as is T_m since it has finite rank). We now compute,

$$\begin{aligned}\mathbb{E}\|T_m - T\|_{HS}^2 &= \mathbb{E}\|\frac{1}{m}\sum_{j=1}^m T^{(j)} - T\|_{HS}^2 \\ &= \mathbb{E}\|\frac{1}{m}\sum_{j=1}^m T^{(j)}\|_{HS}^2 - 2\langle \frac{1}{m}\sum_{j=1}^m \mathbb{E}[T^{(j)}], T\rangle_{HS} + \|T\|_{HS}^2 \\ &= \mathbb{E}\|\frac{1}{m}\sum_{j=1}^m T^{(j)}\|_{HS}^2 - \|T\|_{HS}^2 \\ &= \frac{1}{m}\mathbb{E}_{y\sim\nu}\|T_y\|_{HS}^2 + \frac{1}{m^2}\sum_{j=1}^m\sum_{k\neq j}^m \langle \mathbb{E}[T^{(j)}], \mathbb{E}[T^{(k)}]\rangle_{HS} - \|T\|_{HS}^2 \\ &= \frac{1}{m}\mathbb{E}_{y\sim\nu}\|T_y\|_{HS}^2 + \frac{m^2 - m}{m^2}\|T\|_{HS}^2 - \|T\|_{HS}^2 \\ &= \frac{1}{m}\left(\mathbb{E}_{y\sim\nu}\|T_y\|_{HS}^2 - \|T\|_{HS}^2\right) \\ &= \frac{1}{m}\mathbb{E}_{y\sim\nu}\|T_y - T\|_{HS}^2.\end{aligned}$$

Setting $C^2 = \mathbb{E}_{y\sim\nu}\|T_y - T\|_{HS}^2$, we now have

$$\mathbb{E}\|T_m - T\|_{HS}^2 = \frac{C^2}{m}.$$

Applying Jensen's inequality to the convex function $x \mapsto x^2$ gives

$$\mathbb{E}\|T_m - T\|_{HS} \leq \frac{C}{\sqrt{m}}.$$

$\square$

A.2 Figures of Table 7

Figure 3: $s = 141$

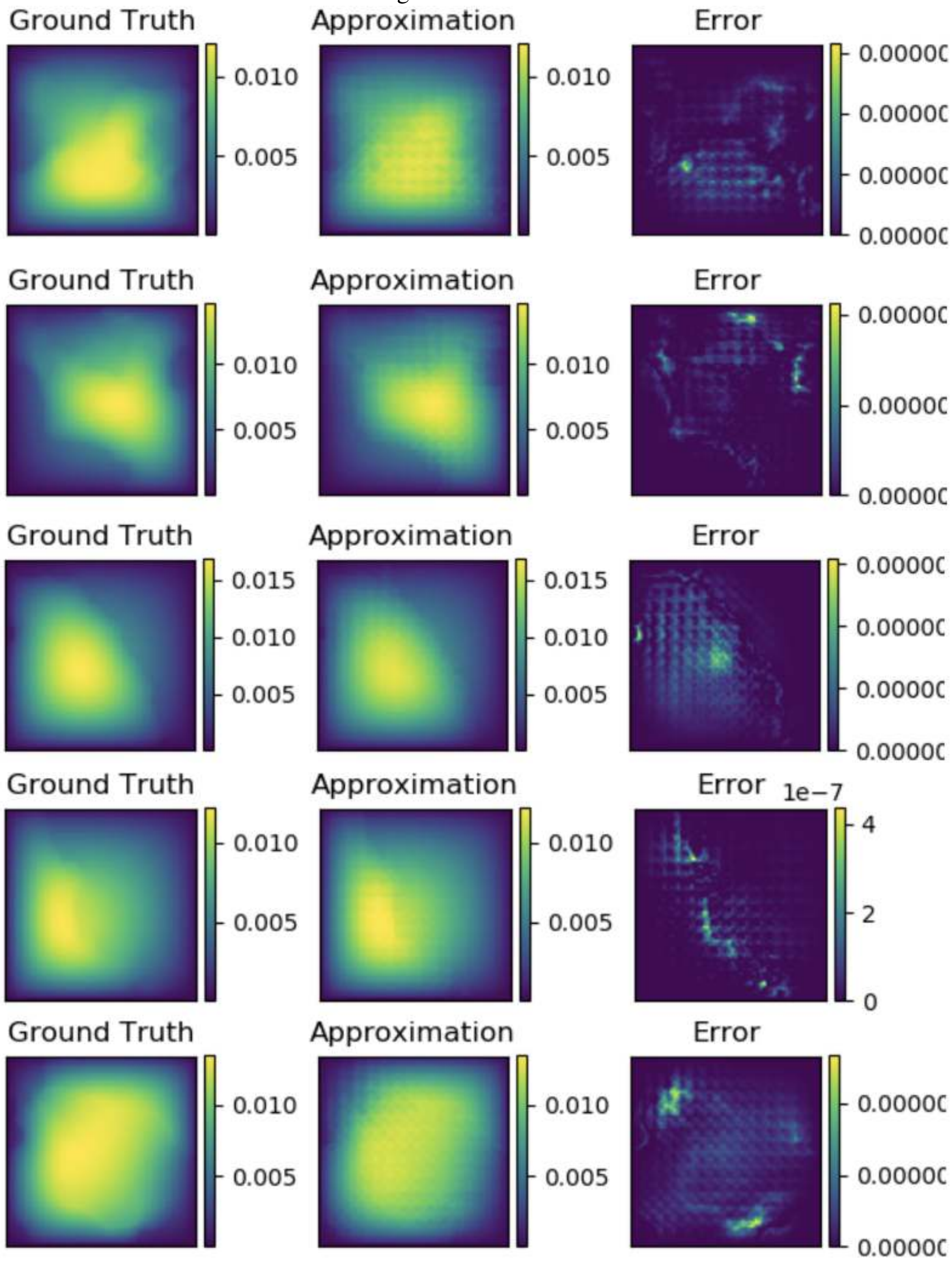

Figure 4: $s = 211$

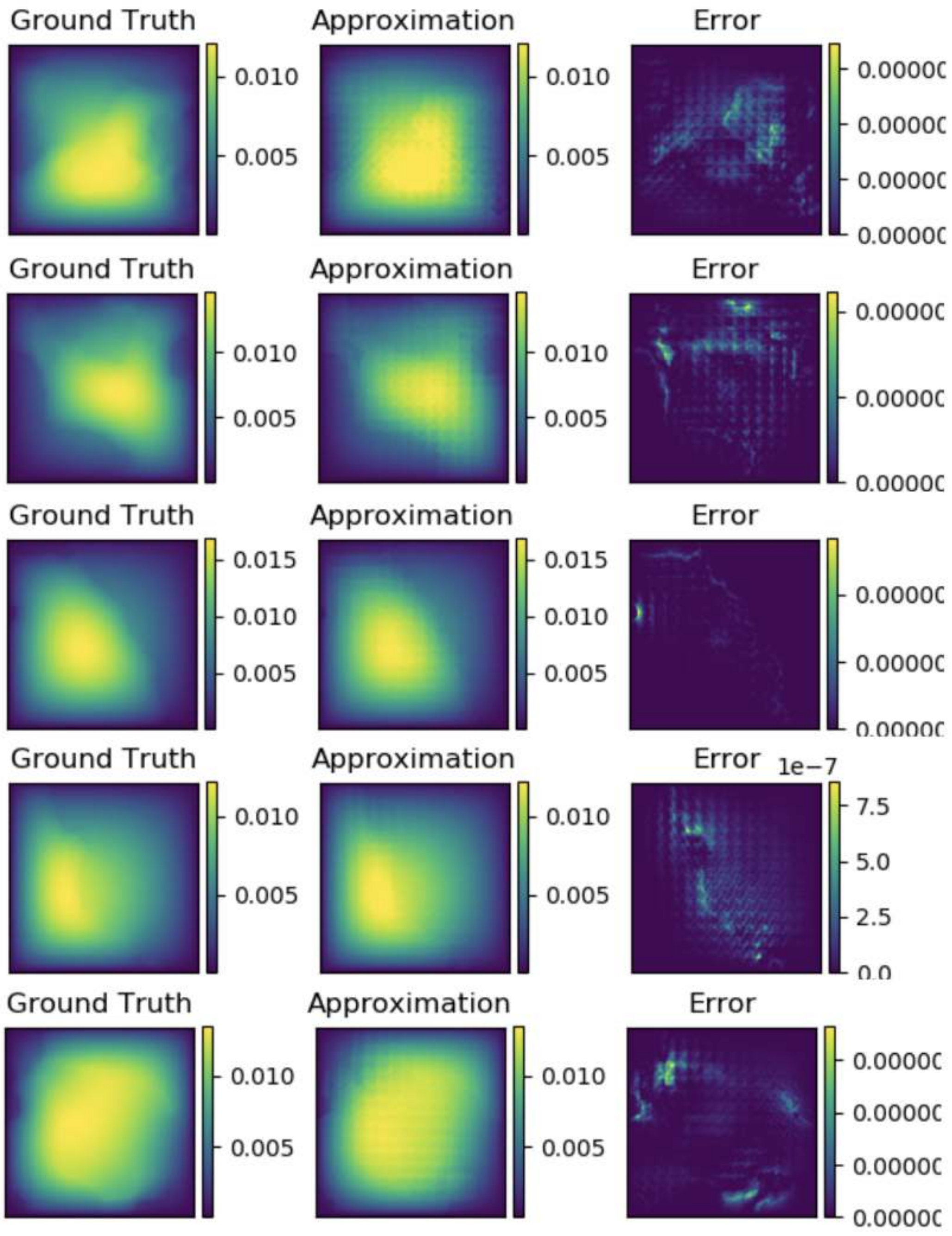

Figure 5: $s = 421$

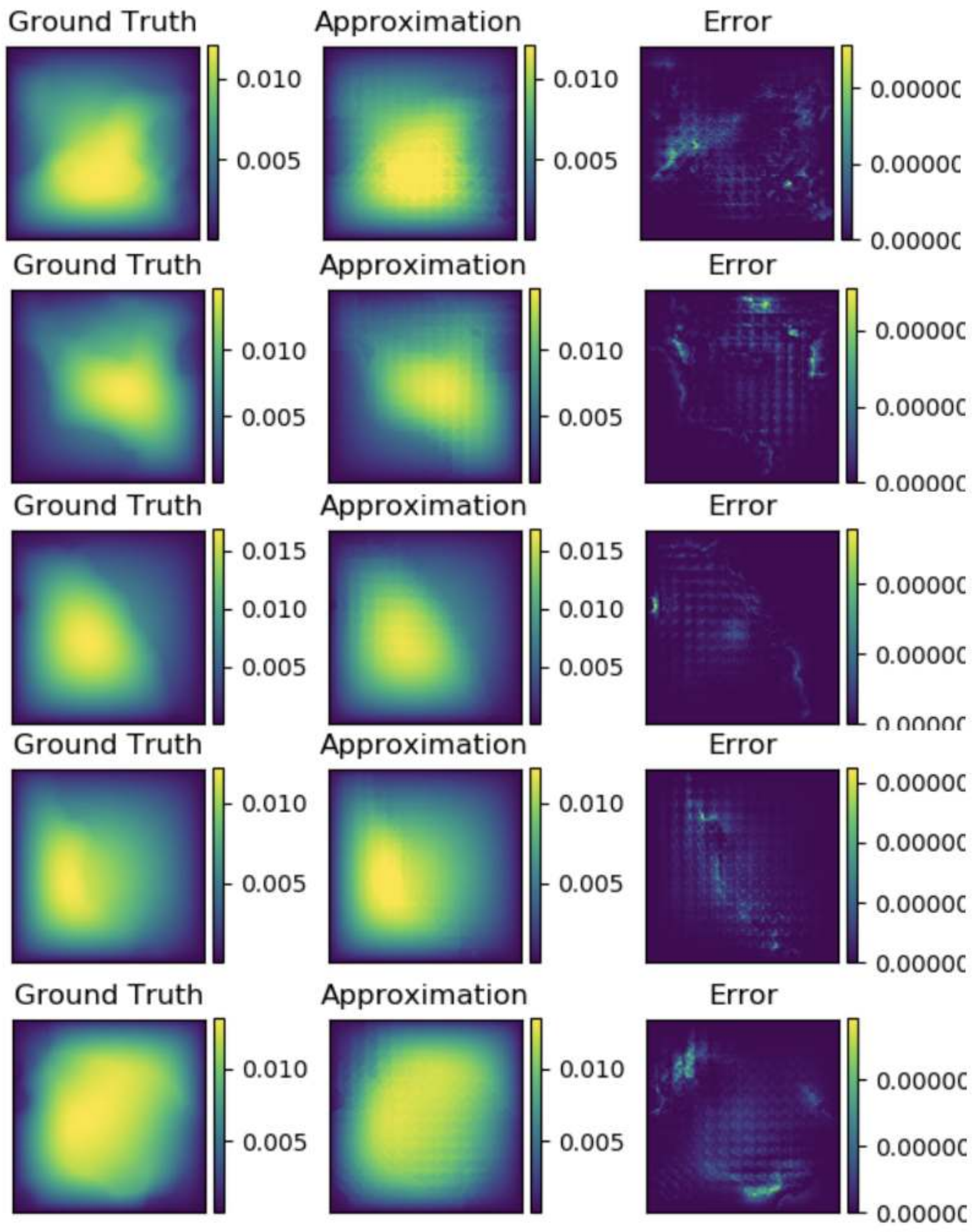
Ground Truth
Approximation
Error